Princeton Plasma Physics Laboratory

PPPL- 4843

PPPL- 4843

Observation of EHO in NSTX and Theoretical Study of its Active Control Using HHFW Antenna

J.-K. Park, et. al.

January, 2013

PPPL PRINCETON PLASMA PHYSICS LABORATORY

Prepared for the U.S. Department of Energy under Contract DE-AC02-09CH11466.

Princeton Plasma Physics Laboratory
Report Disclaimers

Full Legal Disclaimer

Trademark Disclaimer

PPPL Report Availability

Princeton Plasma Physics Laboratory:

http://www.pppl.gov/techreports.cfm

Office of Scientific and Technical Information (OSTI):

http://www.osti.gov/bridge

Related Links:

U.S. Department of Energy

Office of Scientific and Technical Information

Fusion Links

Observation of EHO in NSTX and theoretical study of its active control using HHFW antenna

J.-K. Park,[1] R. J. Goldston,[1] N. A. Crocker,[2] E. D. Fredrickson,[1] M. G. Bell,[1] R. Maingi,[3] K. Tritz,[4] M. A. Jaworski,[1] S. Kubota,[2] F. Kelly,[5] S. P. Gerhardt,[1] S. M. Kaye,[1] J. E. Menard,[1] and M. Ono[1]

[1]*Princeton Plasma Physics Laboratory, Princeton, New Jersey 08543, USA*

[2]*University of California in Los Angeles, Los Angeles, California 90095, USA*

[3]*Oak Ridge National Laboratory, Oak Ridge, Tennessee 37831, USA*

[4]*Johns-Hopkins University, Baltimore, Maryland 21210, USA*

[5]*Unaffiliated*

(Dated: January 9, 2013)

Abstract

Two important topics in the tokamak ELM control, using the non-axisymmetric (3D) magnetic perturbations, are studied in NSTX and combined envisioning ELM control in the future NSTX-U operation: Experimental observations of the edge harmonic oscillation in NSTX (not necessarily the same as EHOs in DIII-D), and theoretical study of its external drive using the high harmonic fast wave (HHFW) antenna as a 3D field coil. Edge harmonic oscillations were observed particularly well in NSTX ELM-free operation with low n core modes, with various diagnostics confirming $n = 4 \sim 6$ edge-localized and coherent oscillations in $2 \sim 8kHz$ frequency range. These oscillations seem to have a favored operational window in rotational shear, similarly to EHOs in DIII-D QH modes . However, in NSTX, they are not observed to provide particle or impurity control, possibly due to their weak amplitudes, of a few mm displacements, as measured by reflectometry. The external drive of these modes has been proposed in NSTX, by utilizing audio-frequency currents in the HHFW antenna straps. Analysis shows that the HHFW straps can be optimized to maximize $n = 4 \sim 6$ while minimizing $n = 1 \sim 3$. Also, IPEC calculations show that the optimized configuration with only 1kAt current can produce comparable or larger displacements than the observed internal modes. If this optimized external drive can be constructively combined, or further resonated with the internal modes, the edge harmonic oscillations in NSTX may be able to produce sufficient particle control to modify ELMs.

I. INTRODUCTION

Edge localized modes (ELMs) can generate unacceptable heat loads to plasma facing components in a reactor scale tokamak or spherical torus, and therefore ELM control is a critical issue in ITER [1, 2]. One of promising and popular concepts is the application of steady non-axisymmetric (3D) fields, which are often called resonant magnetic perturbations (RMPs) since the best ELM control has been achieved especially when the applied 3D field patterns are aligned with the equilibrium magnetic field pitches. The successful RMPs can maintain the pedestal pressure below the edge stability boundary [3–5], as well as to provide sufficient particle transport without ELMs. However, RMP coil requirements for installation are often demanding in cost and engineering, and thus it is also valuable to minimize the coil requirements and/or to find an alternative means of ELM control, such as the operation in the quiescent H (QH) mode [6].

The QH mode utilizes naturally arising 3D fields in the edge, called edge harmonic oscillations (EHOs), instead of externally driven 3D fields in RMP applications. The operational conditions and characteristics have been largely studied recently and reported from DIII-D tokamak. Not many tokamaks however have been successful in the demonstration of the QH mode, and thus it is also critical to produce and test the QH mode in other tokamaks to ensure its scientific feasibility and practicality for ITER. One of important operational aspects is the strong rotational shear, in order to destabilize the peeling-ballooning mode, activate EHOs, and maintain the saturated EHOs to self-regulate the rotational shear [7]. The operational window is correspondingly limited, and unfortunately external 3D field coils are preferred again to control the rotational shear [7, 8]. Nonetheless it should be noted that the 3D coil requirements for the rotation control are less severe than that for RMPs in general, since the toroidal momentum transport is easier to modify than the particle transport. For instance, the pitch-alignment condition for RMPs, which is often claimed necessary to modify the particle transport, requires a narrow spectral peak, and this requirement limits the design choice to an internal coil to be as close as possible to the plasma boundary.

The QH mode operation in DIII-D with I-coil and C-coil shows an example of an indirect but a synergetic combination between internal and external 3D fields. That is, the external I-coil and C-coil fields provide the rotation control to modify the edge stability condition for activating the EHOs, and the internal EHOs provide the particle transport and edge

stability control. The study in this paper proposes another way of a synergetic combination; A direct coupling between the internal and external drive of 3D fields. The externally driven 3D fields should be similar to the internally arising 3D fields in terms of the mode spectrum and frequency to create the resonance and amplification. This direct combination will trade off the operational conditions with the coil requirements, compared with the indirect combination in the DIII-D QH mode or with the RMPs.

Recent NSTX [9] operations provided a very good environment to test and study the possibility of the direct combination, with a number of edge harmonic oscillations observed (not necessarily the same as those observed in the DIII-D QH mode) and with the capability of the high-harmonic fast wave (HHFW) antenna [10] for producing the observed edge harmonic oscillations. This paper will describe first the experimental observations, in Section II, and then the theoretical study of its audio-frequency active control using the NSTX high harmonic fast wave (HHFW) antenna, in Section III. It will also be discussed in Section III if the proposed method can amplify the internally arising harmonic oscillations and possibly provide externally adjustable particle transport and ELM control, with concluding remarks followed in Section IV.

II. OBSERVATION OF EDGE HARMONIC OSCILLATION IN NSTX

Plasma confinement in NSTX has been largely improved with lithium wall coatings with the stabilization of various ELMs. It has been shown that energy confinement time increases and the edge electron thermal diffusivity decreases almost linearly with pre-discharge lithium evaporation rate [11], and that the type-I ELMs can be almost eliminated when the lithium deposition becomes sufficiently strong [12]. If the operational conditions are further adjusted to suppress other small ELMs, such as the type-II or even the type-V, a long ELM-free operation can be achieved in NSTX [13]. Clear edge harmonic oscillations were observed in such an ELM-free condition, reproducibly through a number of discharges.

Figure 1 shows an example, with $\sim 4MW$ of neutral beam injection (NBI) power, $I_P \sim 800kA$ plasma current, and $B_T \sim 4.5kG$. One can see the absence of ELMs during a long period, $t = 0.5s \sim 1s$, from the panel (b), and clear oscillations with low frequency $2 \sim 8kHz$ and intermediate toroidal periodicity $n = 4 \sim 6$ from the panel (d), the Mirnov. The Mirnov coil measurements are specially tuned to low frequency and low amplitudes

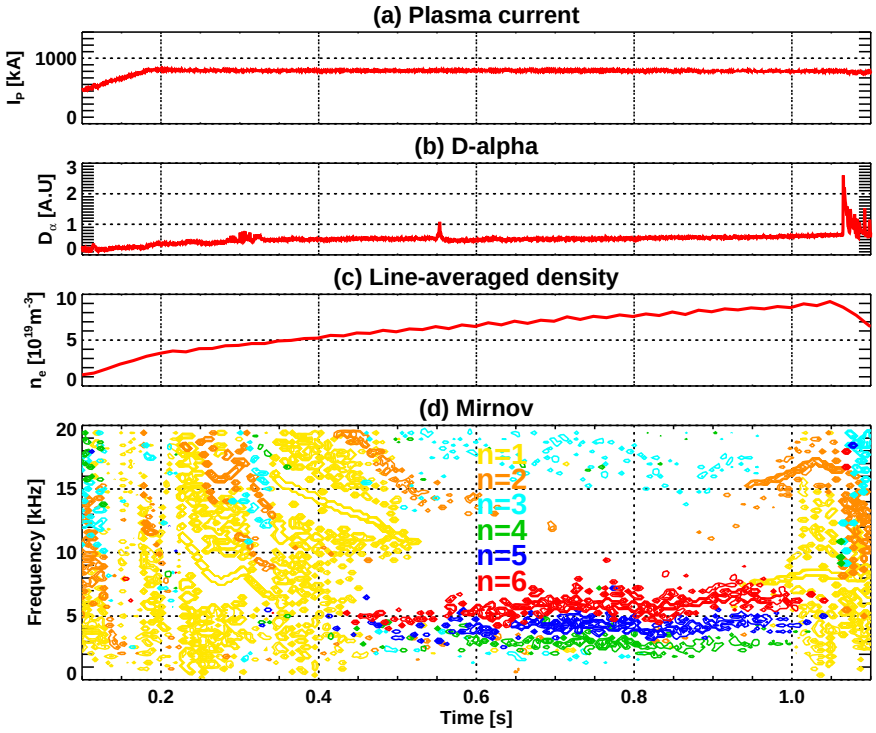

FIG. 1. An example of the edge harmonic oscillations observed in NSTX (#138239). One can see the clearly separated $n = 4 \sim 6$ harmonic oscillations in the ELM-free state at $t = 0.5 \sim 1.0s$, with $2 - 8kHz$ frequency range, from the (d) Mirnov oscillations.

in order to capture the relatively weak amplitudes of the intermediate n modes compared to typical low n mode activities. This long-lived oscillations in fact can be observed in other conditions coincidentally, as reported first from the type-V ELM operating regime [14] with partially similar characteristics, but can be found clearest and strongest in a particular operating condition as described.

The oscillations were also found in other diagnostics, which all suggest the edge-localized and coherent nature of the oscillations. The ultrasoft x-ray (USXR) [15] in Figure 2 (a) used $5\mu m$ of Be foil for the filtering diode array channels, which is the thinner than the conventional $10\mu m$ or $100\mu m$ filters to detect low energy at the end of the pedestal region. One can see that this edge USXR also shows the oscillations in the similar frequency range $2 \sim 8kHz$. Although the oscillations appeared a bit later than the Mirnov due to the difficulty in resolving the weak amplitudes of the intermediate n when the low n modes are active, the three frequency bands are well corresponding to the $n = 4 \sim 6$ modes in the Mirnov after $t = 0.6s$. The oscillations are even stretched out to the far scrape-off layer

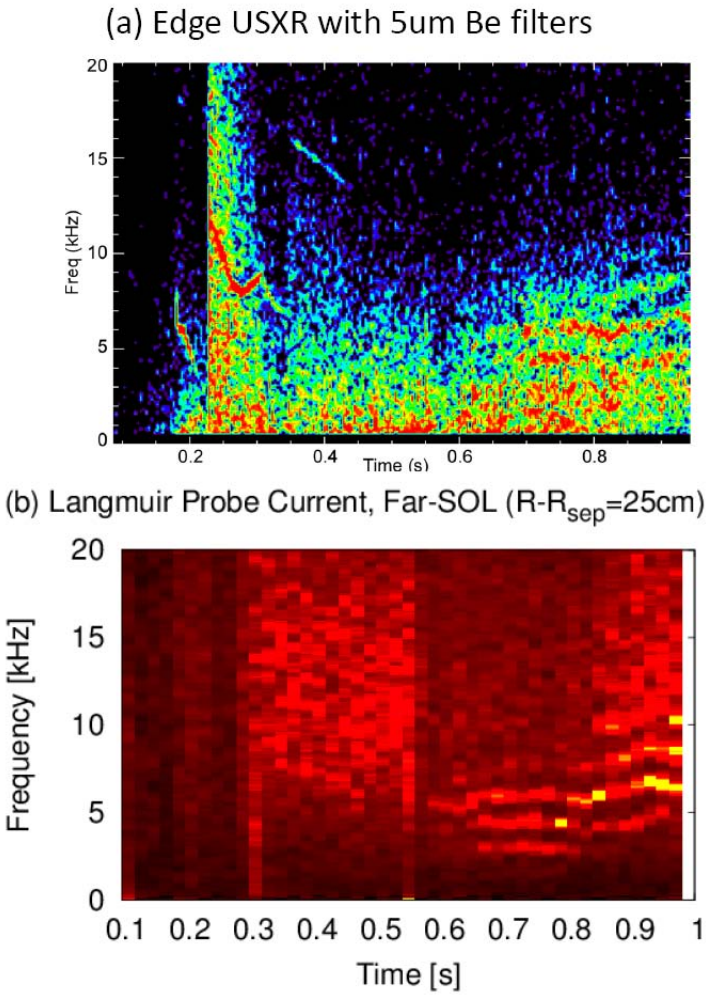

FIG. 2. Edge harmonic oscillations observed in the same discharge #138239 as shown in Figure 1, by (a) the edge USXR, and (b) the Langmuir probes in the far SOL. One can see three bands corresponding to the $n = 4 \sim 6$ in the Mirnov after $t = 0.6s$, in the similar frequency range $2 \sim 8kHz$.

(SOL) region, as shown by the far SOL Langmuir probes [16] in Figure 2 (b).

The edge-localized nature of the oscillations becomes more evident by reflectometer [17], which can resolve the plasma displacement profile by measuring density fluctuations, as shown in Figure 3. One can clearly see the oscillations are localized at $R > 1.35m$, which corresponds to the NSTX pedestal, with the mode amplitudes up to $3 \sim 4mm$. Another observable feature is the coherent nature of the modes. As can be seen from their relative toroidal phases to a toroidal angle reference, Figure 3 (b), the $n > 3$ modes are highly coherent in entire spatial region within only a few %. Note that it is also interesting to see

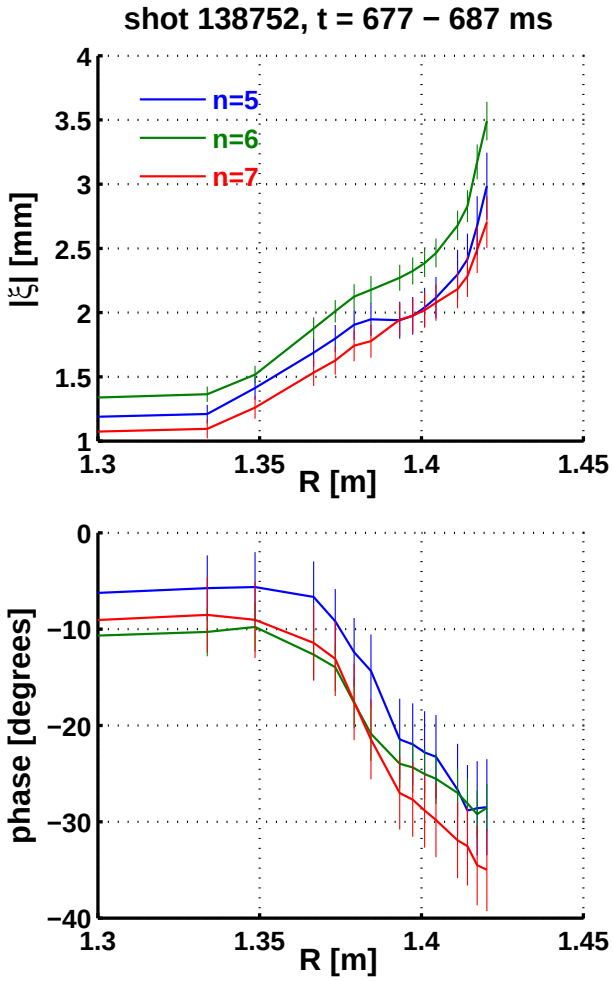

FIG. 3. Plasma displacement profiles associated with the edge harmonic oscillations in NSTX, measured by reflectometer in the discharge #138752. (a) The amplitude shows the edge localized nature and (b) the phase shows the coherent nature of the modes.

the $n > 6$ mode from the reflectometry, while the $n > 6$ is beyond the covering range of the Mirnov. The $n = 6$ mode amplitude is still the largest in the reflectometry, but this $n > 6$ observation indicates that the NSTX edge harmonic oscillations may be the collection of the coherent toroidal harmonic modes covering the wider n than $n = 4 \sim 6$.

Note that these edge coherent, or in other words, edge harmonic oscillations found in NSTX are not necessarily identical to the edge harmonic oscillations (EHOs) in DIII-D driving the QH mode, but seem to have similar stability characteristics. The EHOs on DIII-D are understood as the intermediate n peeling modes destabilized by strong rotational shear and non-linearly saturated by regulating back the rotation shear [7]. The edge harmonic

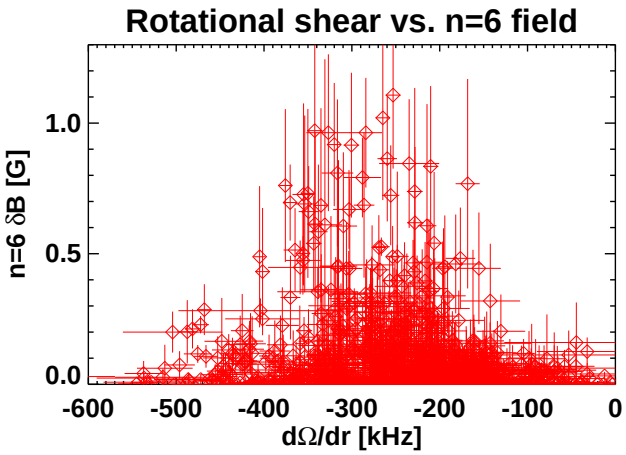

FIG. 4. Statistical analysis indicating the $n = 6$ of the edge harmonic oscillations in NSTX may have a favorable range of the rotational shear.

oscillations in NSTX are also mostly the intermediate n's, indicating that they may also be associated with peeling modes. Moreover, the stability analysis using the DCON code [18] indicates that the studied discharges are close to the marginal stability for $n > 3$ and thus would be easily destabilized if any non-ideal MHD mechanism is involved. In NSTX, the edge harmonic oscillations become apparent in particular operating conditions, such as the beam power $\sim 4MW$ as mentioned earlier in the paper, but those conditions could be favorable to particular kinetic parameters such as the rotational shear. Indeed, although the correlation is not so strong, the statistical analysis for ~ 30 discharges on the Mirnov shows that the $n = 6$ mode amplitudes, for instance, have a favorable range of the rotational shear, as can be seen in Figure 4.

The stability and statistical analysis suggest that the edge harmonic oscillations in NSTX may have similar characteristics to the EHOs in DIII-D. However, these oscillations did not provide any utility on performance in NSTX. For instance, the particle density still kept rising as already shown in Figure 1 (c). That is, the oscillations are coherent and localized in the edge, but the amplitudes are not strong enough to modify the particle or impurity transport. It will be interesting to see if 3D field perturbations can be used to adjust the rotational shear to a favorable level and if the edge harmonic oscillations can be strengthened enough for the particle control, similarly to the non-resonant magnetic field (NRMF) application for the EHOs in the DIII-D QH mode. This can be a good topic to study in the future NSTX-U operation, but here a different utilization of 3D fields will be

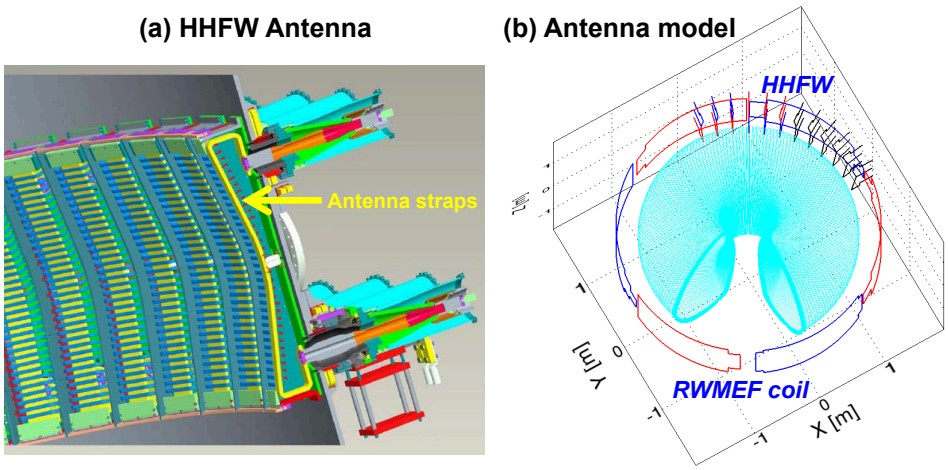

FIG. 5. The actual design of the HHFW antenna in (a), and the filament model of the antenna straps in (b), compared to the existing RWMEF coils. The color codes in (b) actually shows the finally optimized configuration for $n = 4 \sim 6$, as described in the paper.

proposed and discussed. As introduced already, it is a more direct coupling of the external 3D field drive to these naturally arising internal modes, as will be described in the next section.

III. STUDY OF EDGE-HARMONIC MODE CONTROL USING HHFW ANTENNA

The edge harmonic oscillations in NSTX could potentially be used for particle and ELM control if the modes could be amplified by external means such as 3D field coils, directly rather than indirectly, unlike the NRMF control of the rotational shear. It has been proposed that the HHFW antenna can be utilized to couple external 3D fields to the internal modes using audio-frequency currents in the antenna straps. The HHFW antenna locations are localized within a 90 degree toroidal section and so they can effectively drive intermediate n modes in the edge. Figure 5 (a) shows the illustration of the HHFW antenna straps. The straps are composed of 12 toroidal arrays, but each array can be separated through the ground (White) in the middle and so there are 24 straps in total. One can model these HHFW antenna straps with each filament as shown in Figure 5 (b) and treat them as a set of 3D coils. Compared to the existing RWMEF coil, one can see the small apertures, the proximity to the plasma, and the localized nature, indicating the effectiveness for the

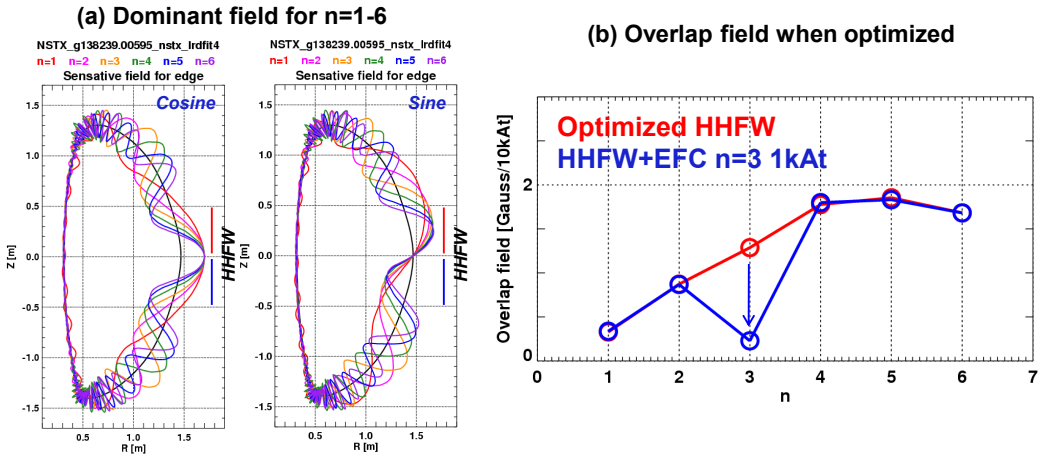

FIG. 6. IPEC analysis for the (a) dominant $n = 1 \sim 6$ external field measured on the plasma boundary, and the (b) overlap with the dominant field when the configuration is optimized for high $n = 4 \sim 6$. In principle, the RWMEF coil can be used to reduce $n = 1 \sim 3$ further, as illustrated in (b).

higher n 3D magnetic perturbations. The straps will be supplied by limited number of power system, and thus the connection and configuration should be optimized.

The optimization should be assessed based on its effectiveness in driving higher $n > 3$ modes while minimizing the low $n = 1 \sim 3$ modes. Our quantification for the optimization is based on the coupling between the dominant mode and the applied field by HHFW straps, for each n. The dominant external field is defined as the field maximizing the resonant responses and can be identified using the Ideal Perturbed Equilibrium Code (IPEC) [19, 20]. Then the coupling with the applied field can be calculated by the overlap integral between the two different field distributions on the plasma boundary. One can define the overlap ratio by $\mathcal{C} = 0 \sim 1$ [21] and also the overlap field by eliminating the normalization. Each configuration gives the overlap field for each n and the effectiveness of the configuration can be assessed by the overlap fields for $n = 4 \sim 6$ while minimizing the overlap fields for $n = 1 \sim 3$.

Figure 6 (a) shows the structure of the dominant external field for each n for the cosine part $C(\theta)$ and the sine part $S(\theta)$ which can be combined to represent the 3D field as $\delta B_n = C(\theta)cos(n\phi) + S(\theta)sin(n\phi)$. One can see that the wavelength, especially of the sine part, becomes comparable to the vertical length of a single strap for higher n, indicating the capability of HHFW straps driving the higher n modes.

The next step is to vary the strap configuration and calculate the applied field and the overlap with the dominant field. Among a number of combinations, additional considerations are (1) assuming just one power supply, which means all the straps should have the same amplitude of currents, and (2) reducing the number of active straps as much as possible to mitigate the voltage requirement. The second consideration is also important for the alternating current drive of the field in the audio-frequency (AC) range for the edge harmonic oscillations, $2 \sim 8kHz$. The HHFW power supply can generate the desired frequency range, but the available current amplitude will be more limited if the targeted frequency and also the number of active straps increase. After the investigation of many different combinations, the optimized configuration could be chosen with the 12 straps and the polarity switch by 3-strap block, as color coded in Figure 5 (b).

The current amplitude will be limited in the high-frequency applications, so it is important to know how much current is actually required to drive the similar amplitude range to the observed mode in the optimized configuration. As the reflectometry provided the information of actual plasma displacements throughout the edge region, IPEC code is used to predict possible range of displacements to be compared with. Figure 7 shows the comparisons for $n = 5, 6$ at the midplane, with $1kAt$ amplitudes for each strap.

Note that the $n = 5$ shows the much stronger plasma amplification than the $n = 6$ in this particular example, but should not be generalized as the high n responses can be sensitive to the profile reconstruction in the edge. One may also be curious about the sharp peaks in the IPEC results. The peaks represent the discontinuity across the rational surfaces due to the ideal constraints. Each rational surface requires the very high and adaptive spatial grid. The total radial grid number is almost up to 10^4 with the poloidal grid up to 10^3 since there are many rational surfaces for a high n for NSTX due to high q_{95}, for example, there are almost 100 rational surfaces for $n = 6$. Therefore, the computational cost is quite demanding even if IPEC is a linear and fast code, and so in fact not many cases were tested. Nevertheless, those other tests showed that the $n = 4 \sim 6$ can vary from the few mm to $\sim 10mm$ depending on the discharge or the reconstruction method. In general, one can conclude that IPEC predicts the larger or at least comparable displacements for the $n = 4 \sim 6$ when the optimized configuration is selected, only with $1kAt$, which is not too demanding to the HHFW power supply in NSTX. Our expectation is that the external drive tuned with the similar amplitude and frequency range may directly amplify the internally

arising modes more than the linear addition via resonance, possibly up to the level that can induce the particle transport and change the edge instability, similarly to the DIII-D EHOs.

It is then also important to ask how much amplification is necessary to cause the particle transport. Although the characteristics of transport and confinement are different between NSTX and DIII-D, one can use the DIII-D EHOs as a reference. The actual field amplitudes estimated for the DIII-D EHOs are up to $\sim 10 Gauss$ [8]. The field amplitudes in the optimized HHFW EHO drive are calculated again by IPEC, as shown in Figure 8 for $n = 5$, as an example. Here the entire $2D$ field structure is shown at a fixed toroidal angle $\phi = 0$ and the displacement structure is also shown for comparison. From the displacement contour, one can obtain Figure 7 along with the midplane. One can see that the field amplitudes already reach to the $\sim 10 Gauss$ only with the $1 kAt$ in the very edge close to the plasma boundary. The predicted $n = 5$ is actually a few times larger than the observed $n = 5$ as shown in the previous Figure 7, which may quantitatively indicate that the naturally arising mode in NSTX is not strong enough to cause the particle transport but that the external

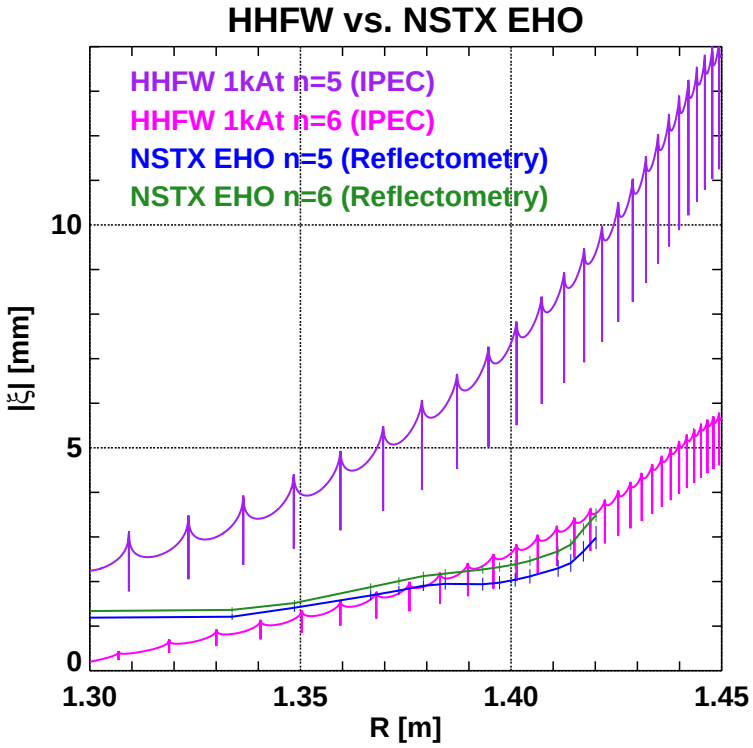

FIG. 7. The externally driven displacements by the optimized HHFW antenna configuration, predicted by IPEC, and the internally driven displacements by the edge harmonic oscillations in NSTX, measured by reflectometry.

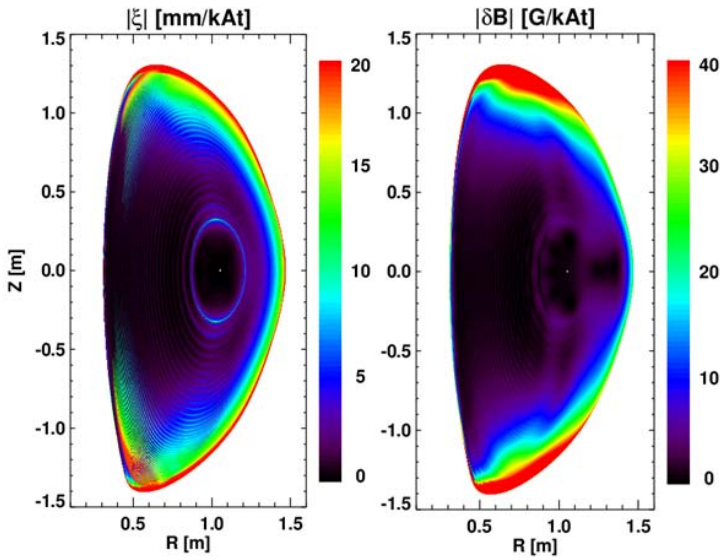

FIG. 8. IPEC prediction for the externally driven $n = 5$ (a) displacements and (b) fields by the optimized HHFW antenna configuration, at $\phi = 0$ position. Only the absolute strength is presented.

drive can possibly amplify the mode up to the required level for the particle transport.

IV. CONCLUDING REMARKS

The observation of the edge harmonic oscillation in NSTX, and the theoretical study of its active drive using HHFW antenna as a 3D coil are presented and discussed. The possibility of implementing a drive system will be examined in NSTX-U first, and successful application may provide a pathway to AC drive of peeling-ballooning modes for edge particle and ELM control in future devices, including ITER. Also, if the externally driven 3D field can be constructively combined with the internally driven oscillations as suggested in this paper, it will be a very useful and unique tool for the ELM control in tokamaks by mitigating the demanding 3D coil requirements and the limited operating conditions, compared to only the external or only the internal 3D field utilization.

This work was supported by DOE Contract No. DE-AC02-09CH11466.

[1] K. Ikeda, Nucl. Fusion **47**, S1 (2007).

[2] R. Hawryluk, D. Campbell, G. Janeschitz, P. Thomas, R. Albanese, R. Ambrosino, C. Bachmann, L. Baylor, M. Becoulet, I. Benfatto, J. Bialek, A. Boozer, A. Brooks, R. Budny, T. Casper, M. Cavinato, J.-J. Cordier, V. Chuyanov, E. Doyle, T. Evans, G. Federici, M. Fenstermacher, H. Fujieda, K. Gal, A. Garofalo, L. Garzotti, D. Gates, Y. Gribov, P. Heitzenroeder, T. Hender, N. Holtkamp, D. Humphreys, I. Hutchinson, K. Ioki, J. Johner, G. Johnson, Y. Kamada, A. Kavin, C. Kessel, R. Khayrutdinov, G. Kramer, A. Kukushkin, K. Lackner, I. Landman, P. Lang, Y. Liang, J. Linke, B. Lipschultz, A. Loarte, G. Loesser, C. Lowry, T. Luce, V. Lukash, S. Maruyama, M. Mattei, J. Menard, M. Merola, A. Mineev, N. Mitchell, E. Nardon, R. Nazikian, B. Nelson, C. Neumeyer, J.-K. Park, R. Pearce, R. Pitts, A. Polevoi, A. Portone, M. Okabayashi, P. Rebut, V. Riccardo, J. Roth, S. Sabbagh, G. Saibene, G. Sannazzaro, M. Schaffer, M. Shimada, A. Sen, A. Sips, C. Skinner, P. Snyder, R. Stambaugh, E. Strait, M. Sugihara, E. Tsitrone, J. Urano, M. Valovic, M. Wade, J. Wesley, R. White, D. Whyte, S. Wu, M. Wykes, and L. Zakharov, Nucl. Fusion **49**, 065012 (2009).

[3] T. E. Evans, R. A. Moyer, P. R. Thomas, J. G. Watkins, T. H. Osborne, J. A. Boedo, E. J. Doyle, M. E. Fenstermacher, K. H. Finken, R. J. Groebner, M. Groth, J. H. Harris, R. J. La Haye, C. J. Lasnier, S. Masuzaki, N. Ohyabu, D. G. Pretty, T. L. Rhodes, H. Reimerdes, D. L. Rudakov, M. J. Schaffer, G. Wang, and L. Zeng, Phys. Rev. Lett. **92**, 235003 (2004).

[4] W. Suttrop, T. Eich, J. C. Fuchs, S. Gunter, A. Janzer, A. Herrmann, A. Kallenbach, P. T. Lang, T. Lunt, M. Maraschek, R. M. McDermott, A. Mlynek, T. Putterich, M. Rott, T. Vierle, E. Wolfrum, Q. Yu, I. Zammuto, H. Zohm, and ASDEX Upgrade Team, Phys. Rev. Lett. **106**, 225004 (2011).

[5] Y. M. Jeon and J.-K. Park, Phys. Rev. Lett. **109**, 035004 (2012).

[6] K. H. Burrell, W. P. West, E. J. Doyle, M. E. Austin, T. A. Casper, P. Gohil, C. M. Greenfield, R. J. Groebner, A. W. Hyatt, R. J. Jayakumar, D. H. Kaplan, L. L. Lao, A. W. Leonard, M. A. Makowski, G. R. McKee, T. H. Osborne, P. B. Snyder, W. M. Solomon, D. M. Thomas, T. L. Rhodes, E. J. Strait, M. R. Wade, G. Wang, , and L. Zeng, Phys. Plasmas **12**, 056012 (1995).

[7] P. Snyder, K. Burrell, H.R.Wilson, M. Chu, M. Fenstermacher, A. Leonard, R. Moyer, T. Osborne, M. Umansky, W. West, and X. Xu, Nucl. Fusion **47**, 961 (2007).

[8] K. H. Burrell, A. M. Garofalo, W. M. Solomon, M. E. Fenstermacher, T. H. Osborne, J.-K. Park, M. J. Schaffer, and P. B. Snyder, Phys. Plasmas **19**, 056117 (2012).

[9] M. Ono, S. Kaye, Y.-K. Peng, G. Barnes, W. Blanchard, M. Carter, J. Chrzanowski, L. Dudek, R. Ewig, D. Gates, R. Hatcher, T. Jarboe, S. Jardin, D. Johnson, R. Kaita, M. Kalish, C. Kessel, H. Kugel, R. Maingi, R. Majeski, J. Manickam, B. McCormack, J. E. Menard, D. Mueller, B. Nelson, B. Nelson, C. Neumeyer, G. Oliaro, F. Paoletti, R. Parsells, E. Perry, N. Pomphrey, S. Ramakrishnan, R. Raman, G. Rewoldt, J. Robinson, A. Roquemore, P. Ryan, S. A. Sabbagh, D. Swain, E. Synakowski, M. Viola, M. Williams, J. Wilson, and the NSTX Team, Nucl. Fusion **40**, 557 (2000).

[10] G. Taylor, R. E. Bell, J. C. Hosea, B. P. LeBlanc, C. K. Phillips, M. Podesta, E. J. Valeo, J. R. Wilson, J.-W. Ahn, G. Chen, D. L. Green, E. F. Jaeger, R. Maingi, P. M. Ryan, J. B. Wilgen, W. W. Heidbrink, D. Liu, P. T. Bonoli, T. Brecht, M. Choi, and R. W. Harvey, Phys. Plasmas **17**, 056114 (2010).

[11] R. Maingi, S. M. K. an C. H. Skinner, D. P. Boyle, J. M. Canik, M. G. Bell, R. E. Bell, T. K. Gray, M. A. Jaworski, R. Kaita, H. Kugel, B. P. LeBlanc, D. K. Mansfield, T. H. Osborne, S. A. Sabbagh, and V. A. Soukhanovskii, Phys. Rev. Lett. **107**, 145004 (2011).

[12] R. Maingi, T. H. Osborne, B. P. LeBlanc, R. E. Bell, J. Manickam, P. B. Snyder, J. E. Menard, D. K. Mansfield, H. W. Kugel, R. Kaita, S. P. Gerhardt, S. A. Sabbagh, F. A. Kelly, , and the NSTX research team, Phys. Rev. Lett. **103**, 075001 (2009).

[13] R. Maingi, A. Hubbard, H. Meyer, J. Hughes, A. Kirk, R. Maqueda, J. Terry, the Alcator C-Mod MAST, and N. teams, Nucl. Fusion **51**, 063036 (2011).

[14] A. Sontag, S. Sabbagh, W. Zhu, J. Menard, R. Bell, J. Bialek, M. Bell, D. Gates, A. Glasser, B. LeBlanc, K. Shaing, D. Stutman, and K. Tritz, Nucl. Fusion **47**, 1005 (2007).

[15] D. Stutman, M. Finkenthal, H. W. Moos, K. B. Fournier, R. Kaita, D. Johnson, and L. Roquemore, Rev. Sci. Instrum. **74**, 1982 (2003).

[16] M. A. Jaworski, J. Kallman, R. Kaita, H. Kugel, B. LeBlanc, R. Marsala, and D. N. Ruzic, Rev. Sci. Instrum. **81**, 10E130 (2010).

[17] N. A. Crocker, W. A. Peebles, S. Kubota, J. Zhang, R. E. Bell, E. D. Fredrickson, N. N. Gorenlenkov, B. P. Le Blanc, J. E. Menard, M. Podesta, K. Tritz, and H. Yuh, Phys. Plasmas **15**, 012303 (2011).

[18] A. H. Glasser and M. S. Chance, Bull. Am. Phys. Soc. **42**, 1848 (1997).

[19] J.-K. Park, A. H. Boozer, and A. H. Glasser, Phys. Plasmas **14**, 052110 (2007).

[20] J.-K. Park, A. H. Boozer, J. E. Menard, and M. J. Schaffer, Nucl. Fusion **48**, 045006 (2008).

[21] J.-K. Park, M. J. Schaffer, R. J. La Haye, T. J. Scoville, and J. E. Menard, Nucl. Fusion **52**, 089501 (2012).

The Princeton Plasma Physics Laboratory is operated
by Princeton University under contract
with the U.S. Department of Energy.

Information Services
Princeton Plasma Physics Laboratory
P.O. Box 451
Princeton, NJ 08543

Phone: 609-243-2245
Fax: 609-243-2751
e-mail: pppl_info@pppl.gov
Internet Address: http://www.pppl.gov